A Model for Designing Ultralow Noise Single- and Dual-Loop 10-GHz Optoelectronic Oscillators

Oriane Lelièvre, Vincent Crozatier, Perrine Berger, Ghaya Baili, Olivier Llopis, Daniel Dolfi, Pascale Nouchi, Fabienne Goldfarb, Fabien Bretenaker, Loïc Morvan, and Grégoire Pillet

***Abstract*—A complete model describing both single- and dual-loop optoelectronic oscillators (OEO) is introduced. It is compared to several experimental configurations, with excellent agreement in all cases. The physical insight into noise coupling mechanisms brought by the model further allows us for the design of ultralow noise OEO. Phase noise performances at 10 GHz with a single 1 km delay line and with a dual 1 km/100 m delay lines are reported. An optimized dual loop configuration exhibits low phase noise floor at high offset frequency (–160 dBc/Hz at 100 kHz) and low spur levels (–145 dBc/Hz), here again in close agreement with our model.**

***Index Terms*—Microwave oscillators, optoelectronic devices, phase noise.**

I. Introduction

OPTOELECTRONIC oscillators (OEO) [1] are able to deliver high purity microwave signals in the 1-10 GHz range. They are low phase noise oscillators directly at high frequencies when other resonator technologies (e.g., quartz crystals, dielectric cavities or acoustic wave resonators) need multiplication stages to reach the GHz range and above. This adding step intrinsically degrades the phase noise performances of these low frequency oscillators.

In a typical OEO [1], the loop consists in a continuous-wave laser modulated by a Mach-Zehnder modulator (MZM), a long fiber-based delay line, and a fast photodiode, which converts the optical modulated carrier into a RF oscillation. This RF signal is further amplified and filtered, before being fed back to the MZM to close the loop. Thanks to low-loss and low-dispersion optical fibers, km-long delay lines can be used, easily providing μs-range delays. For instance, the best performances for a 10 GHz OEO were published using a 16-km-long fiber [2].

Manuscript received April 5, 2017; revised June 15, 2017 and July 7, 2017; accepted July 10, 2017. Date of publication July 18, 2017; date of current version September 8, 2017. This work was supported in part by the Direction Générale de l'Armement. *(Corresponding Author: Oriane Lelièvre.)*

O. Lelièvre, V. Crozatier, P. Berger, G. Baili, D. Dolfi, P. Nouchi, L. Morvan, and G. Pillet are with the Thales Research and Technology, Palaiseau 91120, France (e-mail: oriane.lelievre@thalesgroup.com; vincent.crozatier@thalesgroup.com; perrine.berger@thalesgroup.com; ghaya.baili@thalesgroup.com; daniel.dolfi@thalesgroup.com; pascale.nouchi@thalesgroup.com; loic.morvan@thalesgroup.com; gregoire.pillet@thalesgroup.com).

O. Llopis is with the Laboratoire d'Analyse et d'Architecture des Systèmes, CNRS, Université de Toulouse, Toulouse 31031, France (e-mail: llopis@laas.fr).

F. Goldfarb and F. Bretenaker are with the Laboratoire Aimé Cotton, CNRS – Université Paris Sud – ENS Paris Saclay – Université Paris Saclay, Orsay 91400, France (e-mail: fabienne.goldfarb@u-psud.fr; fabien.bretenaker@u-psud.fr).

Color versions of one or more of the figures in this paper are available online at http://ieeexplore.ieee.org.

Digital Object Identifier 10.1109/JLT.2017.2729018

Nevertheless, reducing the phase noise level of the OEO through an increase of the delay line comes at the expense of several drawbacks. First and foremost, the delay line creates oscillation modes separated by $1/\tau$, where τ is the fiber induced delay. Non-oscillating spectral modes create narrow width high level spurs in the phase noise spectrum. To counterbalance this effect, several delay lines can be implemented in parallel [3] so as to spread the spurs and reduce their height. Other drawbacks will be discussed in the following paragraphs.

As the OEO phase noise performances depend on the components and a few key parameters, simulation is essential to guide the design and the choice of components in order to reach the required performances. The model should include precise characteristics of all the loop components, and their contribution to the overall phase noise spectrum. The first experimental results were fitted with a theoretical study [4], which describes well the low frequency phase noise behavior. More sophisticated models taking into account different noise sources were published [5]–[7], showing good agreement with experimental results over larger bandwidths. Other works focusing on specific noise sources are also available [8], [9]. However these models were developed for single loop OEOs. Multiple loop OEOs are known to degrade the close-to-carrier noise despite providing lower spurs [10]–[12], but, no detailed study agreeing with both low-frequency response and spurs level has been published [7], [13], [14]. In [15], we introduced a preliminary phase noise description for OEOs, which was only tested for a particular dual-loop OEO configuration.

In the present paper, we give a detailed analytical model for OEO phase noise. In Section I, we derive the generic phase noise equations for both single- and dual-loop OEOs. In Section II, we focus on single-loop configuration, with a parametric study of dominant noise sources impact. The Section III is dedicated to dual-loop OEOs. The effect of relative fiber length of both loops is investigated and discussed in terms of close-to-carrier phase noise and spur height reduction. All model predictions are compared to experimental results, with excellent agreement. This exhaustive work allows the design of a 10 GHz dual-loop OEO with state-of-the-art phase noise performances, based on a dual 1 km / 100 m delay line and mostly off-the-shelf components.

II. Modeling of OEO Phase Noise

A. Principle of the Model and Single Loop Case

We derive our phase noise model from the ones described in [16], [17], which are an extension of the well-known feedback

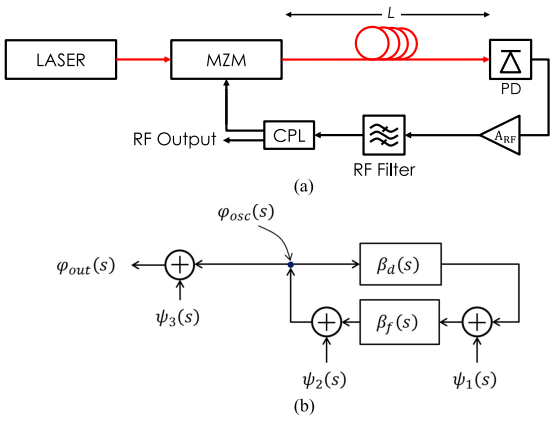

Fig. 1. (a) Schematic setup of a single loop OEO (PD: Photodiode, A_{RF}: RF amplifier, CPL: RF coupler, L: fiber length). (b) Feedback model for the OEO in Laplace domain. ψ_1, ψ_2 and ψ_3 are the phase noise sources.

model from Leeson [18] to the case of OEOs. The principle is to assume that steady-state single-frequency oscillation is reached, and then to establish a closed-loop model for the propagation of phase fluctuations, including the transfer functions of the oscillator elements and the noise sources. By applying the linear feedback theory, the oscillator phase noise is then derived.

If we consider the single loop oscillator architecture depicted in Fig. 1(a), the corresponding closed-loop model in the Laplace domain can be described by the scheme of Fig. 1.(b). In this scheme, φ_{osc} are the phase fluctuations of the circulating signal at the input of the MZM, φ_{out} are the phase fluctuations of the output signal, β_d and β_f are the transfer function of the loop delay and the RF filter, respectively, and $\psi_{1,2,3}$ are the noise sources arising before the filter, after the filter, and at the output respectively.

By examining the feedback scheme, we can state that φ_{osc} must obeys to the relation:

$$\varphi_{osc}(s) = \varphi_{osc}(s)\,\beta_d(s)\,\beta_f(s) + \psi_1(s)\,\beta_f(s) + \psi_2(s) \tag{1}$$

leading to

$$\varphi_{osc}(s) = \frac{\beta_f(s)}{1-\beta_f(s)\cdot\beta_d(s)}\psi_1(s) + \frac{1}{1-\beta_f(s)\cdot\beta_d(s)}\psi_2(s). \tag{2}$$

Equation (2) leads to the following expression for the power spectral density in the frequency domain:

$$S_{\varphi_{osc}}(f) = \left|\frac{\beta_f(2i\pi f)}{1-\beta_f(2i\pi f)\,\beta_d(2i\pi f)}\right|^2 S_{\psi_1}(f) + \left|\frac{1}{1-\beta_f(2i\pi f)\,\beta_d(2i\pi f)}\right|^2 S_{\psi_2}(f). \tag{3}$$

As expected, the model gives the oscillator phase noise power spectral density $S_{\varphi_{osc}}$ as a function of the open loop residual phase noise S_ψ. Indeed,

$$S_{\varphi_{osc}}(f) = \left|\frac{1}{1-\beta_f(2i\pi f)\,\beta_d(2i\pi f)}\right|^2 S_\psi(f), \tag{4}$$

where S_ψ is the open loop phase noise from the MZM input to the coupler output:

$$S_\psi(f) = |\beta_f(s)|^2 S_{\psi_1}(f) + S_{\psi_2}(f). \tag{5}$$

Finally, taking into account the output coupling value, the phase noise at the output of the oscillator is simply given by:

$$S_{\varphi_{out}}(f) = S_{\varphi_{osc}}(f) + S_{\psi_3}(f). \tag{6}$$

We now focus on the transfer functions β_d and β_f. The transfer function β_d for the loop delay corresponds to a time translation, and thus has a simple exponential behavior driven by a time delay τ:

$$\beta_d(2i\pi f) = e^{-2i\pi f\tau}, \tag{7}$$

where the delay τ is the sum of the delay induced by the fiber and the delay τ_{RF} induced by the RF components, i.e., $\tau \cong n_g L/c + \tau_{RF}$, where n_g is the fiber group index at the considered wavelength. It should be noted that the oscillation frequency, that we note f_0, must obey the relation

$$f_0\tau = p, \tag{8}$$

where p is a strictly positive integer linked to the phase part of the Barkhausen condition.

To establish β_f, we assume that it is a single pole Lorentzian bandpass filter. It is the case for high-Q filters based on a single dielectric resonator, frequently used in OEOs due to their narrow bandwidth. We additionally assume that the oscillation frequency is centered relative to the RF filter response. This assumption is easily justified when considering the typical free spectral range of the whole oscillator (few tens to few hundreds of kHz) compared to the typical filter bandwidth (few MHz). That leads to a simple expression for the response to phase fluctuations [16]:

$$\beta_f(2i\pi f) = \frac{1}{1+2iQ_{filter}\frac{f}{f_0}}, \tag{9}$$

where Q_{filter} is the filter quality factor. The next step is to establish the expressions for the noise inputs. The residual phase noise S_{ψ_1}, in rad²/Hz units, has additive and multiplicative parts:

$$S_{\psi_1}(f) = S_{\psi_1,add} + S_{\psi_1,mult}(f), \tag{10}$$

where $S_{\psi,add}$ is the power spectral density corresponding to the incoherent additive noise sources (supposed to be white around the oscillation frequency f_0) and $S_{\psi,mult}$ the power spectral density of multiplicative noise sources, that will be further detailed. Additive noises are the thermal noise N_{th}, the laser relative intensity noise (RIN) at the oscillation frequency $N_{RIN_{HF}}$, and the shot noise N_{shot} detected by the photodiode. As $\psi_1(s)$ corresponds to noise sources after the photodiode, $S_{\psi_1,add}$ is thus given by:

$$S_{\psi_1,add} = \frac{N_{th} + N_{RIN_{HF}} + N_{shot}}{P_{RF}}, \tag{11}$$

where P_{RF} is the RF power at the photodiode output. We have assumed in this last expression that these high frequency noises are equally balanced in phase and amplitude.

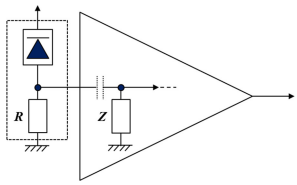

Fig. 2. Resistive matching of the photodiode to the amplifier input impedance Z, i.e., $R = |Z|$ at oscillation frequency.

The RF power at the input of the amplifier is given by:

$$P_{RF} = 1/2 \times R(mI/2)^2 |H_{f_o}|^2, \tag{12}$$

where I is the average photodiode photocurrent, R the photodiode load resistance, m the modulation depth and $|H_{f_0}|^2$ the relative microwave response of the photodiode at the oscillation frequency. The $1/2$ factor on the average photocurrent is due to the resistive matching that we consider between the photodiode and the amplifier (see Fig. 2.).

The thermal noise, high frequency RIN induced noise and shot noise are given by the usual following expressions:

$$\begin{aligned} N_{th} &= k_B T\ NF\ , \\ N_{RIN_{HF}} &= R\ RIN_{f_0}\ \left(I^2/4\right)\ |H_{f_o}|^2, \\ N_{shot} &= 2Re\,(I/4)\,|H_{f_o}|^2, \end{aligned} \tag{13}$$

where k_B is the Boltzmann constant, T the system temperature, e the elementary charge, NF is the noise figure of the RF chain and RIN_{f_0} the relative intensity noise at the oscillation frequency f_0.

Multiplicative noises come from the RF amplifiers and conversion of laser RIN and frequency noise into phase noise by nonlinear processes, so that $S_{\psi,mult}$ is given by:

$$S_{\psi_1,mult}\,(f) = S_{\varphi,amp}\,(f) + S_{\varphi,\,RIN_{LF}}\,(f) + S_{\varphi,f_{opt}}\,(f)\,. \tag{14}$$

In this last expression, $S_{\varphi,amp}$ is the phase noise due to the amplifiers, $S_{\varphi,\,RIN_{LF}}$ is the RF phase noise power spectral density induced by the laser low frequency RIN, and $S_{\varphi,f_{opt}}$ the RF phase noise induced by the optical frequency noise of the laser though fiber dispersion. We have also supposed that all these noise sources are uncorrelated, so that we can simply sum the power spectral densities. $S_{\varphi,amp}$ is the colored part of the RF chain phase noise, that is extracted either from measurements or from the RF amplifiers characteristics provided by the supplier.

$S_{RIN_{LF}}$ is due to the conversion of intensity noise into phase noise by the photodiode nonlinearities [9], that is given by the following expression:

$$S_{\varphi,RIN_{LF}}\,(f) = \chi^2_{phot}\ RIN_{LF}\,(f)\,, \tag{15}$$

where RIN_{LF} is the low frequency RIN spectrum. The intensity to RF phase variations conversion coefficient χ_{phot} strongly depends on the photodiode and its operating point [19]. In our case, the coefficient was measured on an optoelectronic link constituted with the selected OEO components. $S_{\varphi,f_{opt}}$ is given by the following expression:

$$S_{\varphi,f_{opt}}\,(f) = \chi^2_{disp} S_\nu\,(f)\ , \tag{16}$$

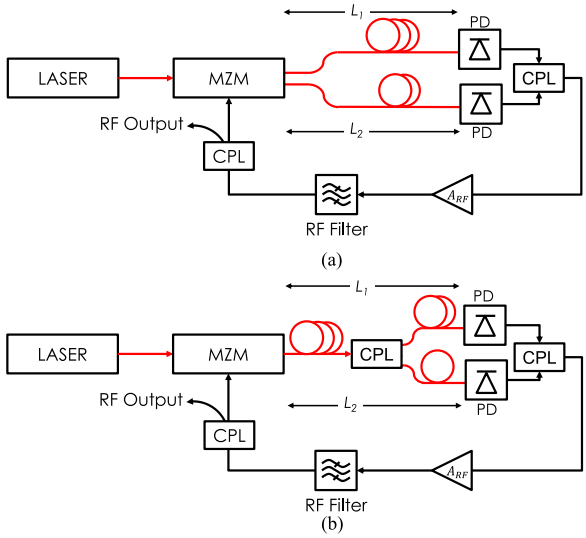

Fig. 3. Configurations of a dual-loop OEO. (a) dual-output MZM case and (b) optical coupler case.

where S_ν is the laser frequency noise power spectral density (PSD). The conversion factor χ_{disp} of the fiber depends on its dispersion D_λ and its length L, and is given by [8]:

$$\chi_{disp} = 2\pi f_0 \lambda_0^2 D_\lambda L/c. \tag{17}$$

Finally, the two last phase noise contributions are

$$S_{\psi_2}\,(f) = k_B\ T/P_{MZM}\,, \tag{18}$$

where P_{MZM} is the RF power at the input of the MZM, and

$$S_{\psi_3}\,(f) = k_B\ T/P_{out}\,, \tag{19}$$

where P_{out} is the oscillator output power.

We will see in part III that this model predicts very accurately the noise of our OEO, either for the low-frequency part and for the spurious level. In the following section, we extend this model to the dual-loop case.

B. Dual Loop Case

The dual loop architecture with two different delays is known to provide a large extinction of the free spectral range spurious [10]–[12]. We thus extend our model to this architecture, distinguishing two configurations. In the first one, a dual output MZM is used to generate the two signals that will experience different delays (Fig. 3(a)), while in the second, a single output MZM is followed by an optical coupler (Fig. 3(b)). In both cases, a 3 dB RF coupler is used to combine the signals from both photodiodes at the input of the RF chain.

To simplify we will now assume that the signal is maximized at the output of the RF coupler. This is usually experimentally obtained with a tunable optical or RF delay line inserted before or after one of the photodiodes, and has the advantage to maximize the signal to noise ratio and the open loop gain. This means that the following relation is satisfied for the delay difference:

$$2\pi f_0\,(\tau_1 - \tau_2) = k + 2\pi q, \tag{20}$$

where τ_1 and τ_2 are the delay induced by the first and second fiber plus the RF delay respectively and $k = \pi/2$ in configuration (a) and $k = 0$ in configuration (b), with q a positive integer. The frequency of oscillation f_0 must also fulfill the Barkhausen condition on the phase, which with (20) reduces to:

$$f_0 \tau_1 = p, \tag{21}$$

with p a positive integer.

To derive the noise of the oscillator, we then use the same relations (3)-(6) as in the single delay case, by only changing the delay transfer function and the noise expressions. Assuming that the two photodiodes exhibit the same transfer function, and that the RF coupler is a 3 dB one inducing no additional phase shift, we can rewrite the delay filtering function for (a) and (b) configurations as:

$$\beta_d\left(2i\pi f\right) = \frac{I_1 e^{-2i\pi f \tau_1} + I_2 e^{-2i\pi f \tau_2}}{I_1 + I_2}, \tag{22}$$

where I_1 and I_2 are the photocurrents on the corresponding photodiodes.

For the noise expressions, it is necessary to write the RF current at the output of the RF coupler in the time domain:

$$i_{RF}\left(t\right) = \frac{m H_{f_o} e^{2i\pi f_0 t}}{2\sqrt{2}} \Big(I_1 e^{-2i\pi f_0 \tau_1 + i\varphi_{b1}(t)} + I_2 e^{i\varphi_{cpl}} e^{-2i\pi f_0 \tau_2 + i\varphi_{b2}(t)} \Big), \tag{23}$$

where i_{RF} is the RF intensity without taking into consideration the RIN and shot noise and $\varphi_{b_{1,2}} \ll 2\pi$ include the contributions from the laser frequency and intensity noises at low frequency. The term φ_{cpl} allows us to take into account the difference between the two configurations. Indeed, in configuration (a), the MZM imposes by principle an opposite RF phase between the two outputs, hence $\varphi_{cpl} = \pi$, while in configuration (b) the optical coupler does not induce any RF phase, i.e., $\varphi_{cpl} = 0$. We have assumed that the modulation index m is the same in the two branches, i.e., the MZM is quadrature biased in configuration (a). From (23), with condition (20), one can derive the signal power at the input of the RF chain:

$$P_{RF} = 1/2 \times R \Big[m\left(I_1 + I_2\right)/2\sqrt{2} \Big]^2 |H_{f_o}|^2. \tag{24}$$

That last expression can be used in (11), provided that we adapt the expressions for the noises. First, we have to take into account that $i_{RIN1,HF}(t)$ and $i_{RIN2,HF}(t)$ are correlated and added up with a delay difference. This leads to the following expression for the RF noise PSD due to the laser RIN at high frequency:

$$N_{RIN_{HF}}\left(f_{RF}\right) = R\, RIN_{f_0}\, |H_{f_0}|^2/8 \times \left(I_1^2 + I_2^2 + 2I_1 I_2 cos\left(2\pi f_{RF}\left(\tau_1 - \tau_2\right)\right)\right). \tag{25}$$

To be inserted in (11), this last expression has to be written for the offset frequency f from f_0, that is quite simple when (20) is satisfied since the RIN is symmetrical around f_0. It leads to:

$$N_{RIN_{HF}}\left(f\right) = R\, RIN_{f_0}\, |H_{f_0}|^2/8 \times \left(I_1^2 + I_2^2 + 2I_1 I_2 cos\left(2\pi f\left(\tau_1 - \tau_2\right) + k\right)\right). \tag{26}$$

It is interesting to note that in configuration (a), the oscillation frequency will correspond to a minimum of the high frequency intensity noise, while in configuration (b) it will correspond to a maximum.

The thermal noise remains the same as in (13) and the shot noise contribution becomes:

$$N_{shot} = 2Re\, \left[\left(I_1 + I_2\right)/4\right]\, |H_{f_o}|^2, \tag{27}$$

Finally, if we examine (23) with condition (20), we can write the signal current as:

$$i_{RF}\left(t\right) = \frac{m H_{f_o} e^{2i\pi f_0 t}}{2\sqrt{2}} \Big(I_1 e^{i\varphi_{b1}(t)} + I_2 e^{i\varphi_{b1}(t)} \Big), \tag{28}$$

That reduces to:

$$i_{RF}\left(t\right) = \frac{m H_{f_o} e^{2i\pi f_0 t}}{2\sqrt{2}} \left(I_1 + I_2\right) e^{i\frac{I_1\varphi_{b1} + I_2\varphi_{b2}}{I_1 + I_2}}, \tag{29}$$

since $\varphi_{b1,2}(t) \ll 2\pi$.

We can then derive the PSD for the low frequency laser noises, that are correlated and added in amplitude with a delay difference $(\tau_1 - \tau_2)$. It leads to:

$$S_{RIN_{LF}}(f) = \left| \frac{I_1 \sqrt{S_{RIN_{LF},1}} + I_2 \sqrt{S_{RIN_{LF},2}}\, e^{2i\pi f(\tau_1 - \tau_2)}}{I_1 + I_2} \right|^2,$$
$$S_f\left(f\right) = \left| \frac{I_1 \sqrt{S_{\varphi,f_{opt1,2}}} + I_2 \sqrt{S_{\varphi,f_{opt1,2}}}\, e^{2i\pi f(\tau_1 - \tau_2)}}{I_1 + I_2} \right|^2. \tag{30}$$

with

$$S_{\varphi,RIN_{LF1,2}}\left(f\right) = \chi^2_{phot1,2}\, RIN_{LF}\left(f\right),$$
$$S_{\varphi,f_{opt1,2}}\left(f\right) = \chi^2_{disp1,2} S_\nu\left(f\right),$$
$$\chi_{disp1,2} = 2\pi f_0 \lambda_0^2 D_\lambda L_{1,2}/c. \tag{31}$$

These new expressions can then be inserted into (14), $S_{\varphi,amp}$ being again obtained from measurements or data on components. The oscillator noise with two delays is then obtained from (3). It should be noticed that compared to [16], our model takes into account the locations of the different input noise sources (amplifier, filter, coupler): it is thus more accurate, specifically for the optimization of the global set-up.

Finally, as we will see in the following paragraphs, it is possible to work with experimental conditions that prevent the occurrence of nonlinear effects such as Brillouin or Rayleigh scattering phenomena, justifying the fact that we did not include them in the model.

C. Multiple Loop Case

To extend this model to a multiple loop case, the dual loop equations can be generalized. Under the same assumptions as

in the dual loop case, we can derive the delay filtering function for a N loop OEO as:

$$\beta_d\left(2i\pi f\right) = \frac{\sum_{q=1}^{N} I_q e^{-2i\pi f \tau_q}}{\sum_{q=1}^{N} I_q}\ , \tag{32}$$

where I_q is the photocurrent on the qth photodiode and τ_q is the delay induced by the qth fiber in the qth loop. Following the same principle, the (24) to (31) can be extended by considering a coherent sum $|\sum_{q=1}^{N} I_q e^{-2i\pi f \tau_q}|^2$ except for (24). In this case, provided that the condition of maximizing the RF combiner output signal is satisfied, a simple sum $\sum_{q=1}^{N} I_q$ can be used. For the shot noise, as expressed in (27), the same sum applies.

Multiple loop OEOs may lead to high spur rejection [3], [14]. However, the requirements to fulfill condition (20) are increasing, requiring a fine adjustment of the multiple delays relative to each other. Experimental validations of these equations are beyond the scope of this paper.

III. Single Loop OEO

In this section, we explain how the model can help to optimize the component selection for ultra-low noise single-loop OEO. We first present the main guidelines and then test the model validity by implementing non optimized components.

A. Selection of the Components

The aim is to design a compact and low noise OEO at 10 GHz. The schematic setup of the single loop OEO is represented in Fig. 1(a). The constraint on the oscillator size forces us to select a compact laser, i.e., a semiconductor laser, and to work with km range fiber length. Despite these two choices, low phase noise levels can be achieved with optimized components. The first step is to optimize the overall RF gain of the microwave link. This means working with a high power photodiode and a low V_π MZM. Unfortunately low V_π MZMs exhibit high optical insertion losses. This latter point can be circumvented by selecting a high power laser. In our case, optical-to-electrical conversion is performed with a high speed photodiode presenting a responsivity of 0.85 A/W. The modulator has a V_π of 1.6 V at 10 GHz and 8 dB optical insertion losses.

The laser should then be selected with respect to its noise contributions. First, as the optical frequency noise is converted into RF phase noise through the optical fiber dispersion as shown in (16) and (17), it should be minimized using a laser with reduced frequency noise and by working either at 1.3 μm, where fiber dispersion is null, or with low-dispersion fibers [8] in the 1.5 μm window. Due to practical considerations, and taking advantage of the low-cost and high performance opto-electronic components used in optical telecommunications, we choose to work at 1.5 μm with km range standard G652 fiber. Second, as the laser intensity noise (RIN) is converted into RF phase noise through the optical-to-electrical conversion as shown in (15), we select a 1.55 μm distributed feedback (DFB) laser exhibiting rather low frequency noise and RIN (see Fig. 4). Its optical output power of 120 mW compensates for the optical losses of the modulator. Its RIN at 10 GHz is measured to be equal to -160 dB/Hz.

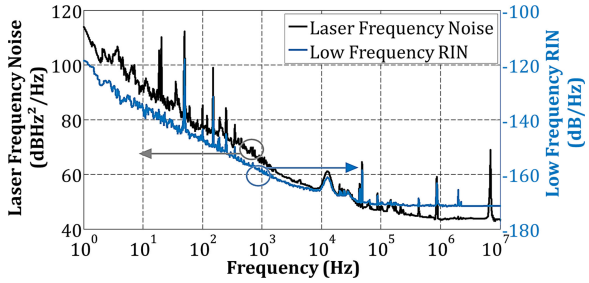

Fig. 4. Measured laser Frequency Noise and low frequency RIN spectra.

The overall filtering function can now be optimized, considering both the fiber length and the RF filter. One has to notice that the fiber length also affects the phase noise induced by the laser frequency noise (see (16)). The model was then use to compute the phase noise with respect to the fiber length, set to 1 km. This optimization is in fact a tradeoff between the spurs frequency and the laser frequency noise contribution as it will be shown in the next section.

The RF filter, on the other hand, has only a filtering role. To achieve the phase noise spectra presented in the next two sections, the RF filter is the unique custom component used in this OEO and it has been internally designed on purpose. It is realized with a high permittivity ceramic rod ($\varepsilon_r = 29.9$) embedded in a copper cavity. A metallic tuning screw at the top allows an adjustment of the frequency. Two small diameter coaxial cables are used for the input/output coupling, with magnetic loops realized at the end of the cables. To isolate the dielectric rod from the copper ground lane, a Teflon spacer is placed in-between. The distances between the resonator and the upper and lower metallic planes are optimized thanks to an analytical model [20] which allows to predict the quality factor and the resonance frequency. The microwave filter has a center frequency of 10.0 GHz with a 4.4 MHz 3-dB bandwidth, 3.8 dB of insertion losses, corresponding to a loaded quality factor Q of 2280.

Knowing all the loss sources, the amplifiers can now be selected. The amplification stage consists here in two 11 dB gain RF amplifiers, providing enough gain for the OEO to oscillate. These amplifiers have been carefully chosen for their low residual phase noise around f_0, i.e., 10 GHz.

Finally, it should be noted that no noises induced by optical nonlinearities, such as Brillouin or Rayleigh scattering, have been taken into consideration in the OEO components selection as well as in our model. Due to the short fiber length, 1 km, and the relatively low optical power in the loop, Brillouin scattering effects are indeed negligible. The most significant remaining noise source induced by a nonlinear effect left is Rayleigh scattering [21]. To efficiently suppress it, we choose to modulate the laser current as suggested in [9], [22]. The modulation frequency was set at 2.5 MHz to not degrade the phase noise spectrum at low frequency offsets.

The open loop phase noise contributions of the selected components are shown in Fig. 5(a). One notices that the laser is the limiting component, both at low frequencies ($<$ 100 Hz) and

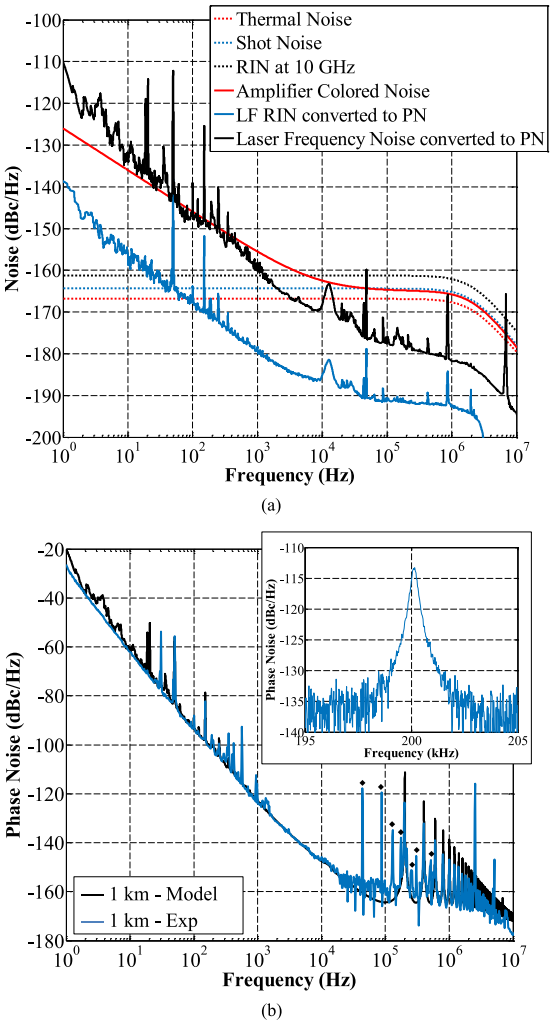

Fig. 5. (a) Open loop phase noise contributions corresponding to the components selection presented in II.A (b) Closed loop phase noise of the single loop OEO at 10 GHz with 1 km delay line (gray/blue line: measurement, black line: model). Black diamonds indicate the spurs caused by the phase noise measurement bench. The inset is a measurement restricted to the first spur, showing the actual level of this spur.

high frequencies ($>$ 10 kHz), because of its frequency noise and 10 GHz RIN, respectively. In between, the amplifier limits the phase noise performances. Thanks to the overall optimization of the RF gain and all the noise consideration when selecting the components, the noise sources are well balanced and will lead to a low phase noise OEO.

B. Experimental Results and Model Validation

Using the components selected above, the OEO is assembled following the set-up described in Fig. 1(a). A typical phase noise spectrum and its prediction by the model are shown in Fig. 5(b). The phase noise measurements were performed using a Keysight E5052B signal-source analyzer. The number of cross correlation was set to 4000 times at 1 Hz in order to get the lowest bench noise floor. As such an acquisition is long ($>$13 h), it is worth mentioning that no control loops were implemented to lock the MZM bias or stabilize the fiber length.

The model expectation fits the experimental phase noise measurement over the full spectral range. Its non-smooth shape is actually due to the measured data that directly feed the simulation (see Figs. 4 and 5(a)). However, some discrepancies can be noticed. First, some peaks, indicated with black diamonds in Fig. 5(b), are not predicted by the model. These peaks are inherent to the measurement bench and were therefore not taken into consideration within the simulation. They are present at the same frequency for all the oscillator setups that we have tested and do not come from the OEO. Second, a difference of 10 dB on the spurs level can be observed. This is due to the too low resolution of the measurement bench, as confirmed by a second measurement, presented in the insert of Fig. 5(b). One can see that with a sufficient resolution, the spur level matches quite well the one predicted by the model. Finally, one can also notice the modulation peak at 2.5 MHz, and its second harmonic, well above the fiber delay line spurs. This peak is due to the laser modulation that suppresses Rayleigh scattering, as explained at the end of the previous section.

As it can be seen in Fig. 5(b), the OEO phase noise has a $1/f^3$ slope from 10 Hz to 5 kHz. This is consistent with the fact that the predominant open loop contributions until 5 kHz are successively the phase noise induced by the laser frequency noise and the RF amplifiers $1/f$ phase noise (Fig. 5(a)).

As previously stated, the 1 km fiber length selection was a trade-off: a longer fiber would have taken the spurs forward with no significant improvement for the low frequency part of the spectrum. To verify these arguments, we experimentally replaced the 1 km delay line with a 4 km delay line. A comparison between the measured phase noise spectrum and the one predicted by the model is presented in Fig. 6(a). As before, the acquisition is obtained by setting the number of cross correlations to 4000 at 1 Hz. This is however not enough to obtain a bench noise floor as low as the noise floor given by the model: this explains the mismatch around 10 kHz that can be observed in Fig. 6(a). The difference on the spur levels is here again due to the resolution of the measurement bench. Despite these remarks, the measurement and the model agree quite well. As predicted, the 4 km long fiber slightly improves the phase noise between 100 Hz and 10 kHz compared to the 1 km case but at the cost of spurs located closer to the carrier. To be more precise, the limiting noise for the lower frequency part of the spectrum is actually the laser frequency noise (see Fig. 5(a)). The use of a longer fiber improves the oscillator filtering function (7) but also increases the laser frequency noise contribution (18) as illustrated in Fig. 6(b). This contribution can be greatly reduced by using dispersion compensated fiber, as stated in Section III-A. However, the implementation of such fibers creates additional optical losses, mainly due to splicing. Consequently another amplifier would be needed to oscillate, cancelling the expected phase noise improvement in the close-to-carrier part of the spectrum. The laser frequency noise problem highlights the interest of a model: understanding the different noise contributions helps to optimize the components, especially when trade-offs have to be found for noise sources depending on the same parameters but with different behaviors.

As mentioned before, the model is directly fed by constructor data or experimental data. But as we are currently not able to measure the amplifier colored noise in the laboratory, this data had to be extrapolated from the datasheet and it can be seen

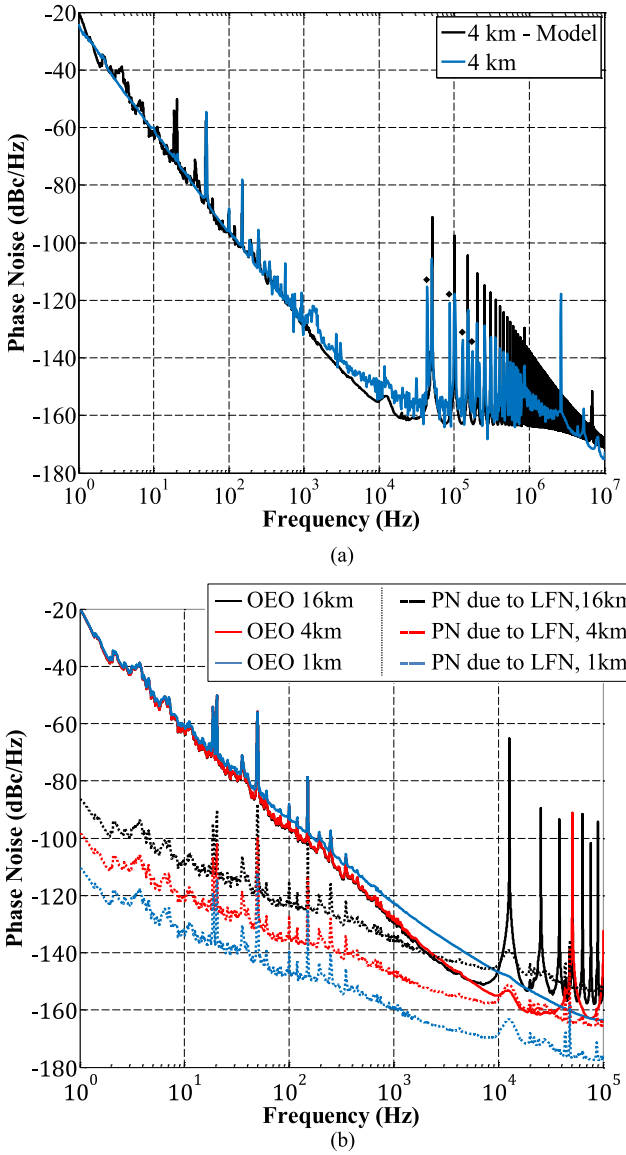

Fig. 6. (a) Phase Noise of the single loop OEO at 10 GHz with 4 km delay line (gray/blue line: measurement, black line: model). Black diamonds indicate the spurs caused by the bench. (b) Phase noise simulation of single loop OEOs at 10 GHz with respectively 1 km, 4 km and 16 km delay line. The dotted lines represent the corresponding open loop phase noise (PN) contributions due to the laser frequency noise (LFN) in each case.

as an adjustment parameter. To verify the model validity, the previously used amplifiers were replaced by a single RF amplifier providing 27 dB of gain. This amplifier is not a low noise amplifier and could be easily characterized. The experimental result for this configuration is presented in Fig. 7. The phase noise spectrum was obtained with only 100 cross correlations at 1 Hz. The good agreement with the model confirms the validity of the previous result. Besides, this measured phase noise spectrum stresses the importance of selecting low noise amplifiers for designing a low noise OEO.

Finally, one can notice that the RF filter was located after the amplifiers: this choice is of importance as it allows us to bend the shape of the noise spectrum in the high frequency domain. In fact, the position of the filter influences (1). In the previous simulations, S_{ψ_1} described all the noises except the thermal noise. When the RF filter is put directly after the photodiode, S_{ψ_1} does not contain the noises induced by the amplifiers: as these noises are not pre-filtered anymore, the phase noise spectrum does not bend anymore in the high frequency domain. To show this effect, two OEO configurations are compared in Fig. 8, with the RF filter placed after and before the amplifiers respectively. The measurements shown in Fig. 8(a) were conducted with 100 cross-correlations at 1 Hz and can be compared with the simulations presented in Fig. 8(b): the very good agreement between the model and the experimental results is again visible. To conclude, using the model described in the first part of this article allowed us to design a simple and compact OEO based on a 1 km standard fiber and mostly standard off-the-shelf components, which provides outstanding noise performances (Fig. 5). In particular the low level of the spurs, –110 dBc/Hz at 200 kHz, is to be emphasized. As a comparison, the low noise OEO described in [8] and based on a DFB laser and 4 km long zero-dispersion fiber has some similarities with the one presented here. But compared to its first spur located at 50 kHz, the spurs of our structure are decreased by 60 dB: thanks to the shorter length of the fiber the frequency of the first spur is pushed in the

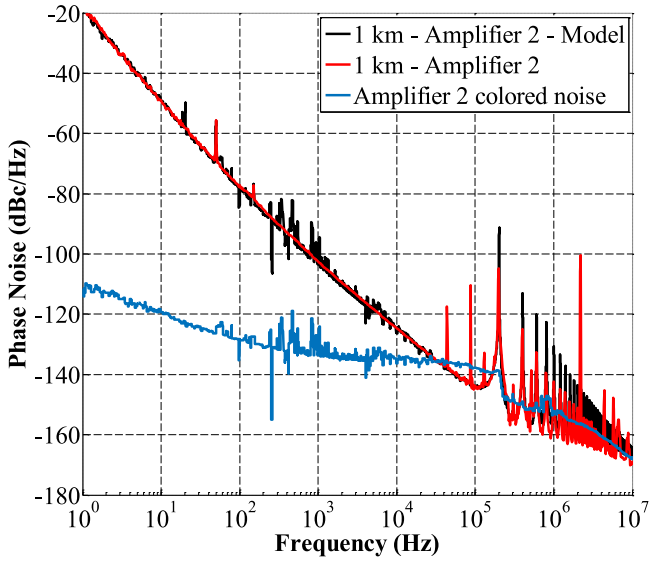

Fig. 7. Phase noise of a single loop OEO at 10 GHz with 1 km delay line using a noisier RF amplifier.

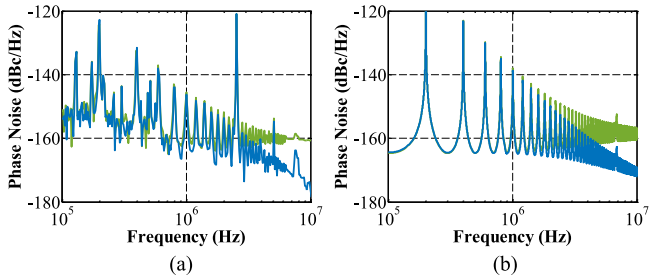

Fig. 8. Influence of the position of the RF Filter on the OEO phase noise (light gray/green line: filter before the amplifiers, gray/blue line: filter after the amplifiers). (a) Measurement (b) Model.

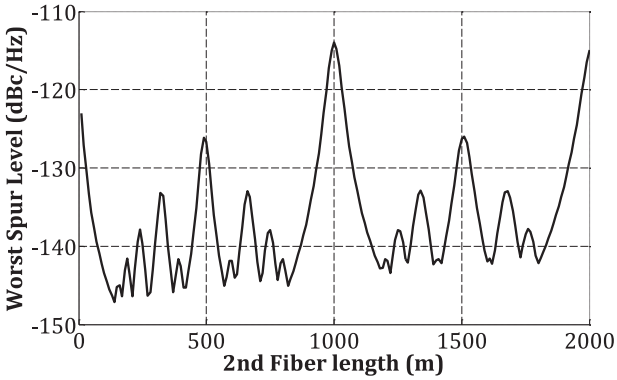

Fig. 9. Simulation of the worst spur level in function of the second fiber length.

cut off bandwidth of the RF filter. Besides, the careful analysis and component selection made through the model allowed to keep similar phase noise results in the low frequency domain.

To carry on the optimization of this structure, two directions can be considered. At low offset frequency, another laser with lower frequency noise could be selected. At higher offset frequencies, a dual loop OEO can be implemented in order to change the oscillator filtering function. This last approach is detailed in the following section.

IV. Dual Loop OEO

In this section, we extend the components selection to a dual-loop case. The model validity will then be tested with two different configurations.

A. Components Selection

In order to compare this OEO to the single loop one and to conclude on the influence of the second loop, we keep all the components already used in the first architecture, including the 1 km fiber. As both outputs of the previously selected MZM are available, there is no need for an optical coupler, thus avoiding additional losses. The signal recombination is simply done with a second photodiode and a 3-dB RF coupler (see Fig. 3(a)). The only parameter left is the second fiber length which can be either chosen to reduce the close-to-carrier phase noise or the spur level. We choose here to decrease the spurs level knowing that the close-to-carrier OEO phase noise can be reduced by using a phase-locked loop [23]. This is in fact a necessity because of long-term frequency considerations before implementing OEOs in real devices. In order to optimize the spurs height, we plot the level of the highest spur, as given by the model, as a function of the second fiber length (Fig. 9 [15]). According to the simulations, the optimum length for the second fiber is 130 meters. In the experiment, we try to approach this value.

B. Experimental Results and Model Validation

To confirm the expectations from the model, the dual loop OEO is characterized in terms of phase noise. For practical reasons, the second fiber length is set to 100 meters; the oscillator should then have a first spur located at 187 kHz with a level

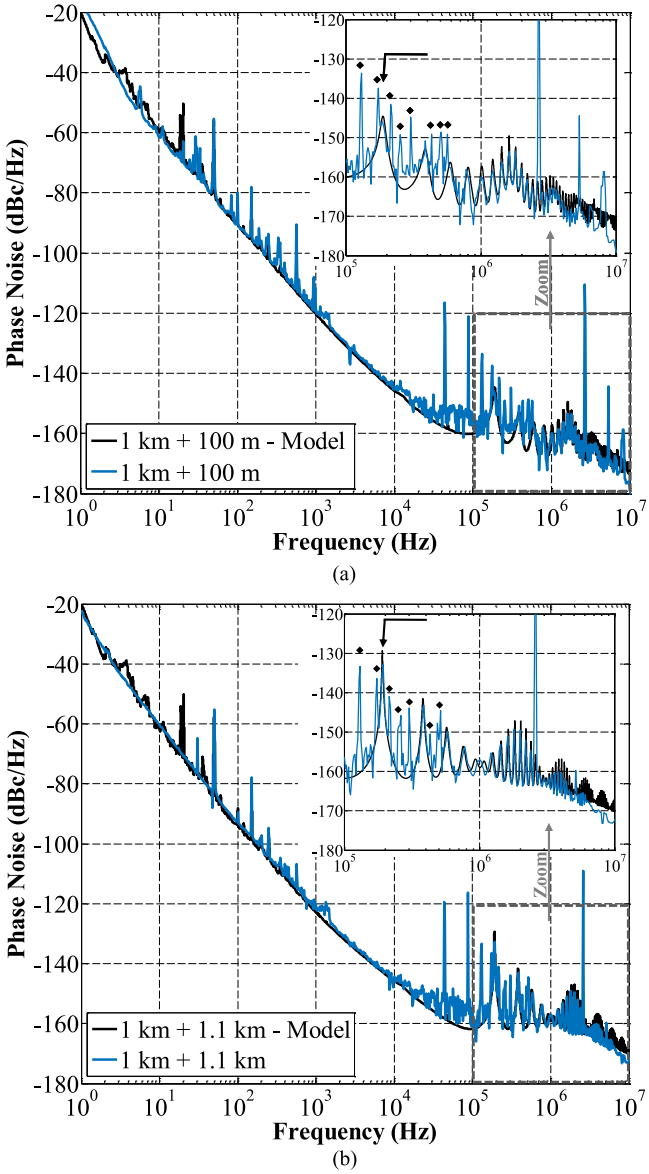

Fig. 10. Phase Noise of the dual loop OEO at 10 GHz with (a) 1 km and 100 m delay and (b) with 1 km and 1.1 km delay lines. In the insets, the black arrow indicates the position of the first spur.

of -145 dBc/Hz. Second, we do not control precisely the fiber lengths, so the condition (22) is not completely fulfilled. However, in our case the OEO noise floor is mainly related to thermal and shot noises, so the delays related parts in (25) and (30) are almost negligible in the phase noise.

The number of cross correlations is set to 1000 at 1 Hz, and no control loops were implemented to lock the MZM bias and stabilize the fiber lengths. Typical phase noise spectra are presented in Fig. 10. The dual loop OEO exhibits phase noise levels of -119.5 dBc/Hz at 1 kHz and -145 dBc/Hz at 10 kHz. The first spur is located at 187 kHz with a noise level equal to -145 dBc/Hz. Due to the addition of the 100-m-long fiber, the spurs in the dual loop case are wider than in the single loop case. In this case, the resolution of the bench is now sufficient and the measured width matches the model prediction (Fig. 10(a)).

Compared to the single loop case, one can notice that the dual-loop configuration slightly degrades the phase noise in the low frequency domain (Fig. 5(b)), as predicted above. However, the additional 100 m delay line reduces the spur height by 35 dB. Furthermore, the phase noise degradation close-to-carrier was limited to a few dB thanks to the careful components selection. Compared to the literature, these results outperform other published results of multiple loop 10 GHz OEOs [11]–[13].

In order both to propose a dual loop OEO with a better close-to-carrier noise and to test the model with other configurations, we studied a dual loop OEO with a much longer delay line. This second dual loop OEO follows the setup presented in Fig. 3(b) and has respectively 1 km and 1.1 km fiber length on each loop. A few dB should be gained on the phase noise for the lower frequency offsets but, according to Fig. 9, at the cost of higher spurs. This is confirmed by the phase noise spectrum in Fig. 10(b), which shows again the good agreement between the phase noise spectra obtained by measurement and by simulation.

Despite higher spurs, this last configuration presents the lowest off-the-carrier phase noise at 10 GHz for a dual loop OEO. These results show how important the use of a model is when aiming to design low noise oscillators, specifically when trade-offs have to be made between the spur and low frequency noise levels.

Finally, the simulated phase noise was integrated between 1 kHz and 10 MHz to obtain the RMS jitter in both dual loop cases and in the 1 km single loop OEO case. Using the simulated results prevents from integrating measurement artifacts (e.g., resolution). The good agreement between experimental data and simulations allows the use of simulated data for jitter extraction. The RMS jitters are equal to 0.72 fs, 0.94 fs and 1.68 fs for the 1 km / 100 m OEO, the 1 km / 1.1 km OEO and the 1 km OEO respectively. In the best case scenario, the 1 km / 100 m dual loop OEO reduces by a factor 2 the RMS jitter of its single loop counterpart. These results further emphasize the reason why spur height is critical when aiming for a high purity signal.

V. Conclusion

In conclusion, we have presented a complete model working for both single and dual loop OEOs. We used it to design two compact OEO configurations, with respectively 1 km and 1 km / 100 m delay lines, mostly composed of standard off-the-shelf components and without any special effort on integration (no fiber stabilization, no bias control of the MZM). These OEOs exhibit extremely low phase noises (-123 dBc/Hz and -119.5 dBc/Hz at 1 kHz, and -145.8 dBc/Hz and -145 dBc/Hz at 10 kHz for the single loop OEO and dual loop OEO respectively). In particular, the spur levels obtained with the two OEO architectures are significantly improved in comparison to other publications. Moreover, the low-frequency phase noise degradation in the dual-loop architecture is minimized, which makes it attractive for many applications. In both cases, the laser is the limiting component, because of its frequency noise. These results highlight the simplicity of the OEO concept for the generation of high spectral purity RF oscillators in the high frequency domain.

Acknowledgment

The authors would like to thank the Direction Générale de l'Armement for their fruitful discussions.

References

[1] X. S. Yao and L. Maleki, "Converting light into spectrally pure microwave oscillation," *Opt. Lett.*, vol. 21, pp. 483–485, 1996.
[2] D. Eliyahu, D. Seidel, and L. Maleki, "Phase noise of a high performance OEO and an ultralow noise floor cross-correlation microwave photonic homodyne system," in *Proc. 2008 Int. Symp. IEEE Freq. Control*, 2008, pp. 811–814.
[3] X. S. Yao and L. Maleki, "Multiloop optoelectronic oscillator," *IEEE J. Quantum Electron.*, vol. 36, no. 1, pp. 79–84, Jan. 2000.
[4] X. S. Yao and L. Maleki, "Optoelectronic microwave oscillator," *J. Opt. Soc. Amer. B*, vol. 13, no. 8, pp. 1725–1735, 1996.
[5] E. C. Levy, M. Horowitz, and R. M. Curtis, "Modeling optoelectronic oscillators," *J. Opt. Soc. Amer. B*, vol. 26, no. 1, pp. 148–159, 2009.
[6] Y. K. Chembo, E. Larger, E. Rubiola, K. Volyanskiy, and P. Colet, "Determination of phase noise spectra in optoelectronic microwave oscillators: A Langevin approach," *IEEE J. Quantum Electron.*, vol. 45, no. 2, pp. 178–186, Feb. 2009.
[7] K. Volyanskiy, "The study of phase noise spectra of a microwave delay line optoelectronic oscillator," Ph.D. dissertation, Dept. Eng. Sci., Université de Franche-Comté, Besançon, France, 2009.
[8] K. Volyanskiy, Y. K. Chembo, L. Larger, and E. Rubiola, "Contribution of laser frequency and power fluctuations to the microwave phase noise of optoelectronic oscillators," *J. Lightw. Technol.*, vol. 28, no. 18, pp. 2730–2735, Sep. 2010.
[9] D. Eliyahu, D. Seidel, and L. Maleki, "RF amplitude and phase-noise reduction of an optical link and an opto-electronic oscillator," *IEEE Trans. Microw. Theory*, vol. 56, no. 2, pp. 449–456, Feb. 2008.
[10] P. Devgan, "A review of optoelectronic oscillators for high speed signal processing applications," *ISRN Electron.*, vol. 2013, 2013, Art. no. 401969.
[11] W. Zhou, O. Okusaga, C. Nelson, D. Howe, and G. Carter, "10 GHz dual loop opto-electronic oscillator without RF amplifiers," *Proc. SPIE Optoelectron. Integr. Circuits X*, vol. 6897, no. 68970Z, pp. 1–6, 2008.
[12] D. Eliyahu and L. Maleki, "Tunable, ultra-low phase noise YIG based Ooto-electronic oscillator," in *Proc. Int. Symp. IEEE MTT-S Microw. Dig.*, 2003, vol. 3, pp. 2185–2187.
[13] T. Bánky, B. Horváth, and T. Berceli, "Optimum configuration of multiloop optoelectronic oscillators," *J. Opt. Soc. Amer. B*, vol. 23, no. 7, pp. 1371–1380, 2006.
[14] D. Eliyahu and L. Maleki, "Low phase noise and spurious level in multiloop opto-electronic oscillators," in *Proc. 2003 Int. Symp. IEEE Freq. Control*, 2003, pp. 405–410.
[15] O. Lelièvre *et al.*, "Ultra low noise 10 GHz dual loop optoelectronic oscillator: Experimental results and simple model," in *Proc. 2016 Int. Symp. IEEE Freq. Control.*, 2016, pp. 1–5.
[16] S. Römisch, J. Kitching, E. Ferrè-Pikal, L. Hollberg, and F. L. Walls, "Performances evaluations of an OEO," *IEEE Trans. Ultrason., Ferroelectr., Freq. Control*, vol. 47, no. 5, pp. 1159–1165, Sep. 2000.
[17] E. Rubiola, *Phase Noise and Frequency Stability in Oscillators*. New York, NY, USA: Cambridge Univ. Press, 2009.
[18] D. B. Leeson, "A simple model of feedback oscillator noise spectrum," *Proc. IEEE*, vol. 54, no. 2, pp. 329–330, Feb. 1966.
[19] Z. Abdallah *et al.*, "Photodiode nonlinear modeling and its impact on optical links phase noise," in *Proc. Int. Conf. Eur. Freq. Time Forum*, 2014, pp. 48–51.
[20] D. Kajfez and P. Guillon, *Dielectric Resonators*. Norwood, MA, USA: Artech House, 1986.
[21] A. Docherty, C. R. Menyuk, J. P. Cahill, O. Okusaga, and W. Zhou, "Rayleigh-scattering-induced RIN and amplitude-to-phase conversion as a source of length-dependent phase noise in OEOs," *IEEE Photon. J.*, vol. 5, no. 2, Apr. 2013, Art. no. 5500514.
[22] J. P. Cahill, W. Zhou, and C. Menyuk, "Additive phase noise of fiber-optic links used in photonic microwave-generation systems," *Appl. Opt.*, vol. 56, no. 3, pp. B18–B25, 2017.
[23] Y. Zhang, D. Hou, and J. Zhao, "Long-term frequency stabilization of an optoelectronic oscillator using phase-locked loop," *J. Lightw. Technol.*, vol. 32, no. 13, pp. 2408–2414, Jul. 2014.

Authors' biographies not available at the time of publication.